Low-Profile Wideband Circularly Polarized Array Antennas Using Integrated Half-Power Quadrature Power Divider

Lehu Wen, Steven Gao, *Fellow, IEEE*, Qi Luo, *Senior Member, IEEE*, Wei Hu, *Member, IEEE*, Benito Sanz-Izquierdo, and Xue-Xia Yang, *Senior Member, IEEE*

***Abstract*—Low-profile wideband circularly polarized (CP) array antennas using integrated half-power quadrature power divider (HP-QPD) are presented. A novel HP-QPD is first proposed as an important design concept for CP radiation. Detailed analyses show that the proposed HP-QPD can have half-power CP radiation and the remaining half-power transmission with equal-magnitude but quadrature phase difference. Therefore, it can be utilized for designing a 1×2 CP array antenna. Compared to the traditionally designed single-feed or dual-feed CP counterparts, this 1×2 array antenna can have more than four times wider axial ratio (AR) bandwidth with three CP modes and a simple feed network. This 1×2 array antenna was then designed, fabricated, and measured for performance verification. Both measured and simulated results show that this array antenna can have a wide overlapped impedance and AR bandwidth of 7.9% with a thin dielectric thickness of $0.031\lambda_0$. The 1×2 array antenna was further extended to a 1×8 linear array antenna for high gain CP radiation. Measured results show that unidirectional and symmetrical radiation patterns are achieved with high peak realized gain of 15.4 dBic, low profile, and simple feed network.**

***Index Terms*—Circular polarization, half-power quadrature power divider, patch antenna, wideband antenna.**

I. Introduction

CIRCULARLY polarized (CP) antennas have the advantages of reduced multi-path fading effect and flexible antenna orientation compared to the linearly polarized antennas in wireless communication systems. Therefore, they have been widely applied in the high sensitivity and long distance transmission required wireless application scenarios, such as electronic toll collection (ETC), radar, satellite, and navigation systems [1]. In these different applications, because of the increasingly limited and valuable installation space, CP antennas with wide operation bandwidth, low profile, and low fabrication cost are very appealing.

This work was supported by Engineering and Physical Sciences Research Council under Grant EP/N032497/1, Grant EP/P015840/1, and Grant EP/S005625/1. *(Corresponding author: Lehu Wen.)*

L. Wen, S. Gao, and B. Sanz-Izquierdo are with the School of Engineering and Digital Arts, University of Kent, Canterbury, CT2 7NT, U.K. (e-mail: L.Wen@kent.ac.uk)

Q. Luo is with the School of Physics, Engineering and Computer Science, University of Hertfordshire, Hatfield, AL10 9AB, UK.

W. Hu is with the National Key Laboratory of Antennas and Microwave Technology, Xidian University, Xian, 710071, China.

X.-X. Yang is with the School of Communication and Information Engineering, Shanghai University, 200444, China.

Traditionally, crossed dipoles [2]-[10] are commonly used for wideband CP radiation. For this type of antennas, how to introduce quadrature phase delay between the orthogonally arranged dipoles is a key factor to determine CP performance. Simply, one can use a narrow circular strip [2] or a series feed line [3]-[4] as a 90° phase delay line. By elaborately adjusting the characteristic impedance of series microstrip line [4], a wide CP bandwidth of 41.3% is achieved. In addition, novel transmission lines of using slow-wave delay lines [5] and composite right-hand and left-hand transmission lines [6] are presented for quadrature phase shift. In [6], when right-hand and left-hand transmission line unit cells are introduced on the dipole arms, low axial ratio (AR) of less than 1.7 dB is measured with a wide bandwidth of up to 53.4%. A novel wideband half-power phase shifter using open slot [7] is proposed and utilized for CP radiation with the AR bandwidth of 55.6%. CP radiation can also be realized by using multi-feed method in [8]-[10] with very wider AR bandwidth of 96%. However, to achieve unidirectional radiation and wide CP bandwidth, antennas of this kind normally require a large reflector and high profile to maintain a stable radiation and a wide operation bandwidth.

To obtain low profile and compact size, patch antennas [11]-[23] are normally utilized for realizing CP radiation. Traditionally, by introducing protruded stubs [11], etched slots [12], or shorted vias [13], two orthogonal modes with quadrature phase difference on a same patch can be generated for CP radiation. Because of the simple single-feed method, these antennas usually have a narrow CP bandwidth. Therefore, dual-feed [14]-[16] and four-feed [17]-[20] methods are utilized for CP bandwidth improvement. In [14], quadrature phase is obtained through two different aperture coupling paths, and wideband AR bandwidth of 11.5% is achieved. A new four-feed structure using shorted loop is presented in [17], and wideband compact 4×4 array antenna is realized for CP radiation. By interlacing feed networks and sharing adjacent patches, dual CP array antenna is developed with a reduced element spacing [21]. In these antennas, due to the additional wideband quadrature feed network, wide AR bandwidth can be ensured. However, insertion loss and manufacture cost will be increased. Above from the independently designed CP antenna elements, series-fed CP patch antennas [22]-[24] are researched for high integration and innate beam scanning performance. However, their available bandwidths are normally limited by the series-fed method, and the directional radiation patterns vary with the working frequency.

In this work, two highly integrated wideband CP patch array antennas are presented, which are aimed to cover the frequency band of 5.7-5.9 GHz with the gain higher than 14 dBic for ETC applications. A novel half-power quadrature power divider (HP-QPD) is first proposed as a key component for wideband CP array design. It can not only radiate half-power right-hand CP (RHCP) waves to the free space, but also transmit equal magnitude but quadrature phase energy to the output ports. Working principle of the proposed HP-QPD is detailed discussed and illustrated. Based on this HP-QPD, a 1×2 CP array antenna is presented with a simple feed network but a wide CP bandwidth with three CP modes. More than four times bandwidth enhancement is achieved compared to the traditionally designed single-feed or dual-feed CP antennas. Finally, a linear array antenna with 1×8 elements are designed for high gain applications. Both the 1×2 and 1×8 linear array antennas were fabricated and measured for performance verification. Measured results show that the 1×2 array antenna has a wide bandwidth of 8% for $|S_{11}|$<-10 dB and AR<3 dB using a thin dielectric with the thickness of $0.031\lambda_0$. The 1×8 linear array antenna has a high gain of 15.4 dBic and an overlapped bandwidth of 7.4%. Owing to the low-profile structure, it can be easily flush-mounted into an installation surface for wireless communications.

II. Half-Power Quadrature Power Divider

A novel half-power quadrature power divider (HP-QPD) is proposed and illustrated in this section. It can radiate half-power RHCP radiation to the free space, and output the remaining half-power energy with equal magnitude and quadrature phase difference. This component works as an important basis for the design of wideband CP patch array antennas.

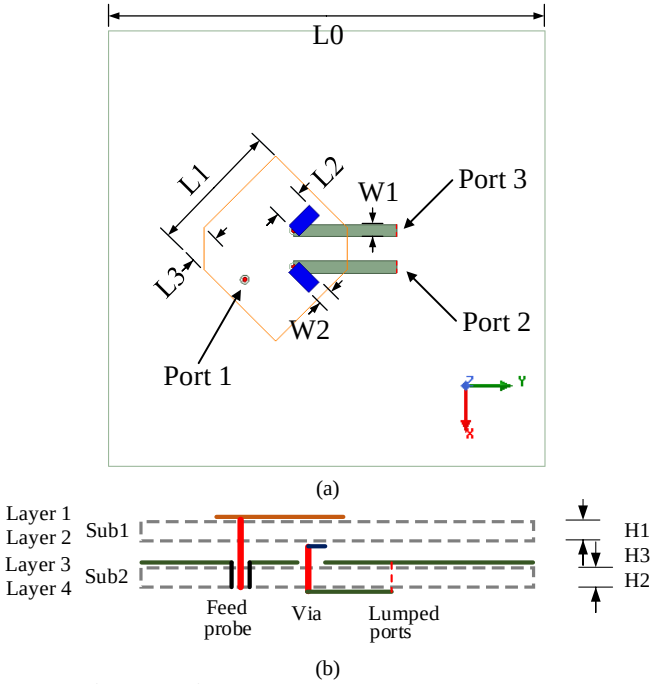

Fig. 1. Configuration of the proposed HP-QPD. (a) Top view. (b) Side view. (Detailed design parameters, L0=60mm, L1=18 mm, L2=4 mm, L3=4 mm, W1=1.7 mm, W2=2 mm, H1=H2=0.813 mm, H3=0.8mm.)

Fig. 1 shows the detailed configuration of the proposed HP-QPD. As shown in Fig. 1 (a), this HP-QPD is composed of a top radiating patch with the contour line shown in orange color, a small rectangular strip shown in blue color for proximity coupling, and a pair of microstrip feed lines shown in navy color for quadrature output. The top radiating patch is in a square shape with a pair of opposite corners chamfered. A feed probe is located along φ=-45° direction, and denoted as the input port 1. Two lumped ports are placed at the end of the microstrip lines for quadrature output, and denoted as output port 2 and port 3. Utilizing the above configuration, half-power input energy will be radiated in the form of RHCP wave, and the remaining half-power energy will be transmitted evenly to the two output ports with a quadrature phase difference.

Fig. 1 (b) shows the side view of the proposed HP-QPD, which gives the stack details of each layer. Here, two substrates of Rogers 4003C with the relative permittivity of 3.55 and thickness of 0.813mm are used in the HP-QPD design. An air gap with the thickness of 0.8 mm is set between the two substrates, so there are four conducting layers in the design. Detailed design parameters are listed in the caption of Fig. 1. All simulated results in this work are obtained from the commercial EM simulation software Ansys HFSS 2019.

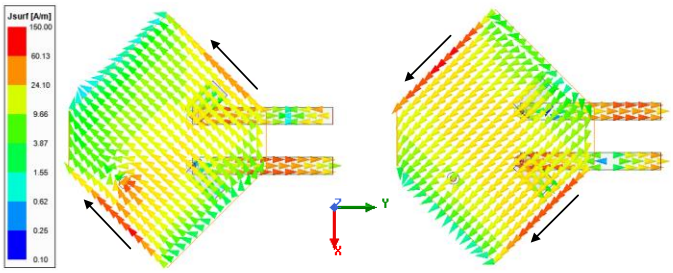

Fig. 2. Current distributions on the surface of the proposed HP-QPD. (a) t=T/4, (b) t=T/2.

When port 1 is excited, the top radiating patch works as a single feed CP antenna for RHCP radiation. Simultaneously, port 2 and port 3 achieve an equal magnitude but sequential quadrature output. Fig. 2 shows the current distributions on the surface of the proposed HP-QPD at different times of a period T, where T is the oscillation period at the operation frequency of 5.8 GHz. It can be seen that at time t=T/4, the current direction on the patch is along φ=-135° direction. When time comes to t=T/2, the current direction is in φ=-45° direction. Therefore, RHCP radiation is realized on the chamfered square patch.

Another important phenomenon is that the parallel microstrip lines can be sequentially excited with quadrature phase difference. At the time t=T/4, strong current distribution is found on the lower microstrip line, while week current distribution is observed on the upper microstrip line. When the time comes to t=T/2, current distributions on these two microstrip lines are exchanged. Strong current distribution is found on the upper microstrip line, while week current distribution is observed on the lower microstrip line. Note that current distributions at the times t=3T/4 and t=T are almost same as the current distributions at the times t=T/4 and t=T/2,

except the inverse current directions on the conductor surface. So they are not included in the figure for brevity.

Fig. 3 shows the S-parameter responses of the proposed HP-QPD. As shown in Fig. 3 (a), port 2 and port 3 can get equal magnitude output at around 5.8 GHz, which is close to -6 dB. This means that half energy will be radiated to the free space, and the other half energy will be transmitted to two output ports. In addition, a good input impedance is achieved from 5.6 GHz to 6.4 GHz with the reflection coefficient less than -10 dB. Phase responses of S_{21} and S_{31} are shown in Fig. 3 (b). It can be seen that port 3 has a negative phase delay compared to port 2. At around 5.75 GHz, the delayed phase difference between port 2 and port 3 is -90°. Therefore, it can be expected that, when a dual-feed CP antenna is connected to these two ports, another CP mode can be excited at this frequency.

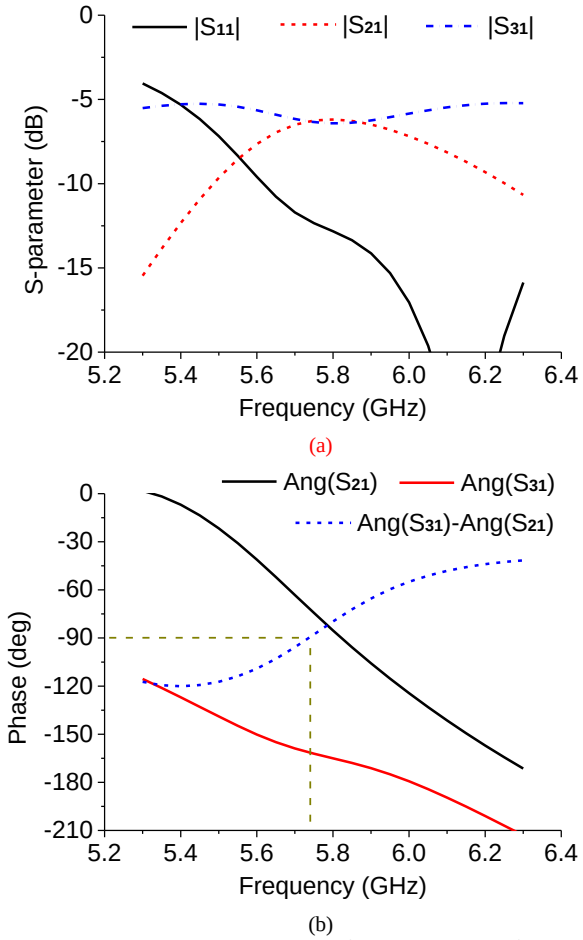

Fig. 3. Magnitude and phase responses of the S-parameters for the proposed HP-QPD.

Now considering an ideal case that a dual-feed CP antenna is connected to the HP-QPD. If defining the output characteristics of the proposed HP-QPD as

$$\frac{S_{21}}{S_{31}} = Me^{j\phi} \tag{1}$$

where S_{21} and S_{31} are the transmission coefficients of the HP-QPD, M and ϕ is the magnitude and phase of the related complex ratio. Supposing that all output ports are connected to the ideal dual-feed CP antenna without mismatching, one can get that an estimated AR radiated from the connected ideal dual-feed CP antenna [2] is

$$AR = \sqrt{\frac{1 + M^2 + \sqrt{1 + M^4 + 2M^2\cos(2\phi)}}{1 + M^2 - \sqrt{1 + M^4 + 2M^2\cos(2\phi)}}} \tag{2}$$

Fig. 4 compares the estimated AR using (2) and the radiated AR from the top radiating patch. It can be seen that the estimated AR bandwidth (AR<3 dB) calculated from the output characteristic of HP-QPD is wider than the radiated AR bandwidth. In addition, it can be seen that two CP modes are not coincident at the same frequency. The minimum of the estimated AR is located at 5.75 GHz, while the minimum of the radiated AR is located at 5.8 GHz. This slight discrepancy can be utilized to produce two CP modes and obtain a wide AR bandwidth. Observing from results shown in the figure, it can be concluded that at least two CP modes can be obtained if a dual-feed CP antenna connects to the output ports of HP-QPD. It will be one CP mode is from top radiating patch, the other CP mode is from the external connected dual-feed CP antenna.

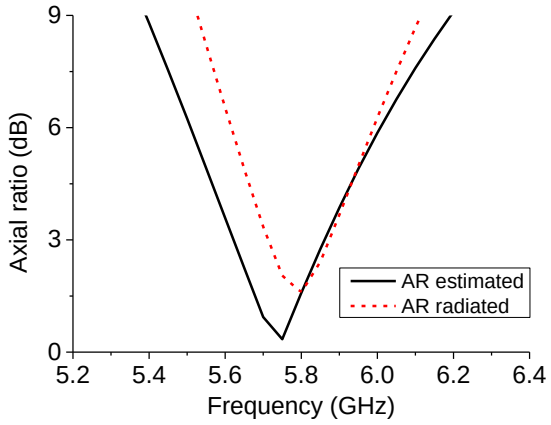

Fig. 4. Estimated AR and radiated AR of the proposed HP-QPD.

In the design of HP-QPD, parameters of the corner chamfer (L3) and the coupling strip (L2) can have important effects on the output characteristics. Fig. 5 shows the magnitude and phase responses of HP-QPD vary with these two design parameters. It should be noted that when one parameter is studied, the other parameters keep unchanged as listed in the caption of Fig. 1.

As shown in Fig. 5 (a), when the chamfered length increases from 3.5 mm to 4.5 mm, more energy is transmitted to into port 2, and less energy is transmitted into port 3. When L3 equals 3.5 mm, curves of S_{21} and S_{31} are intersected at the center. When L3 increases to 4.5 mm, two curves are departed. It means that magnitude imbalance will happen at the two output ports when L3 deviates from its optimal value. Another important effect is that the corner chamfer can also have a great effect on the delayed phase difference between the two output ports. It can be seen that, when L3 is increased, more delayed phase difference can be obtained.

Fig. 5 (b) gives the magnitude and phase responses vary with different lengths of the coupling strip (L2). It can be observed that, when L2 is decreased to 3 mm, the transmitted energy at port 2 and port 3 is reduced. When L2 is increased, more energy

will be transmitted to port 2 and port 3. Therefore, the coupling strip under the radiating patch can be used to control the total output magnitude at the two output ports. In addition, the delayed phase difference shows that, no matter how L2 changes, the phase difference between the two output port is nearly unchanged, which keeps stable at -90° at the frequency of 5.75 GHz, and this frequency is close to the resonating frequency of the top radiating patch. Therefore, based on the above parametrical studies, it is not difficult to achieve equal magnitude close to -6 dB, and quadrature phase difference between two output ports for the proposed HP-QPD.

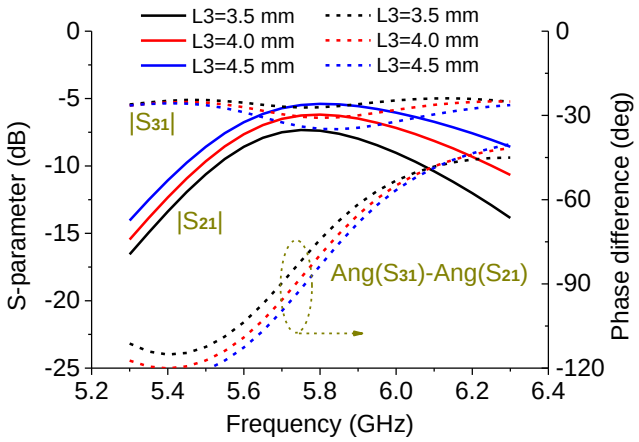

Fig. 5. Magnitude and phase responses of the proposed HP-QPD vary with different parameters. (a) Different chamfered lengths (L3). (b) Different coupling lengths (L2).

III. 1×2 CP Array Antenna

Based on the above analyses on HP-QPD, it is expected that a wide CP bandwidth can be achieved with at least two CP modes when a dual-feed CP antenna is connected to HP-QPD. Therefore, in this section, a wideband 1×2 CP array antenna is proposed and demonstrated based on this design concept.

A. Array Configuration

Fig. 6 shows the configuration of the proposed 1×2 CP array antenna using the integrated HP-QPD. The structure of HP-QPD is almost the same as the structure shown in Fig. 1 except some slight changes of the dimensions for the overall optimal CP performance. A microstrip feed line is extended to the left edge of the substrate for a SMA side connection. A dual-feed CP antenna is connected to the ends of two output feed lines. The top radiating patch of the dual-feed CP antenna is in square shape with the length of L4. The left dual-feed CP antenna is also excited by using the proximity coupling method with a small rectangular strip. To achieve unidirectional CP radiation in the broadside direction, the length of the microstrip feed line between HP-QPD and dual-feed CP antenna (L6) is designed as one guided wavelength in the substrate. Detailed design parameters are listed in the caption of Fig. 6 for the ease of reference.

Fig. 6 (b) shows the side view of the 1×2 CP array antenna. The stack configuration is same as the design in Fig. 1 (b). Two substrates of Rogers 4003C with the thickness of 0.813 mm are used in the design, and an air lay with the thickness of 0.8 mm are used to separate these two substrates. One should be noticed that for the convenience of soldering, all via holes in this design penetrate through the first layer to the fourth layer. Each top radiating patch has an etched circle for isolating the conducting via hole.

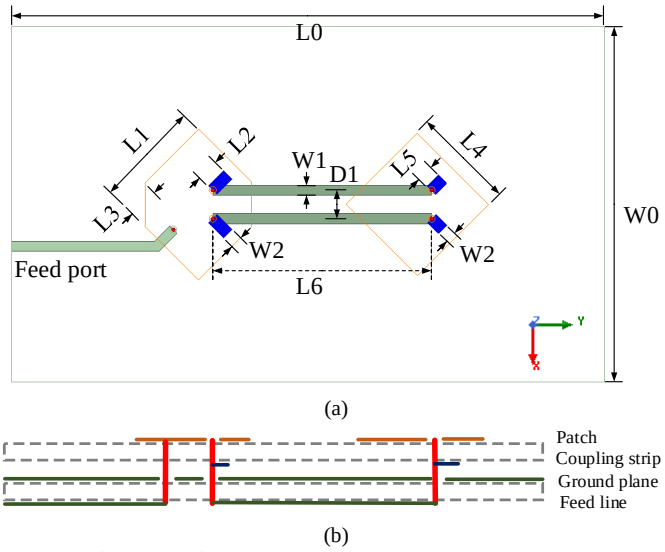

Fig. 6. Configuration of the proposed wideband CP 1×2 array antenna. (a) Top view. (b) Side view of the radiator. (Detailed design parameters, L0=100 mm, L1=18 mm, L2=1.3 mm, L3=5.3 mm, W0=60mm, W1=1.7 mm, W2=2 mm, L4=17 mm, L5=1.4 mm, L6=36.9 mm, D1=4.8 mm, H1=H2=0.813 mm, H3=0.8mm.)

B. Antenna Study

The proposed 1×2 CP array antenna elaborately incorporates a single-feed CP antenna using direct probe feed and a dual-feed CP antenna using proximity coupling feed, but obtains a much wider overlapped AR and impedance bandwidth compared to these two kinds of the traditionally designed antennas. Fig. 7 shows the comparison between the proposed antenna and two traditionally designed CP antenna examples. It should be noted that to be fair, the design of reference Antenna 1 and Antenna 2 have the same substrate and layer configuration as the proposed antenna, and they are optimized to get the AR bandwidth as wide as possible.

As shown in the figure, the simulated CP bandwidth (AR<3 dB) for the proposed 1×2 CP array antenna is 5.54-5.99 GHz (7.8%) with three AR minima at 5.58 GHz, 5.78 GHz, and 5.95 GHz respectively. Three CP modes are obtained and radiated for the proposed antenna. The impedance bandwidth for $|S_{11}|$<-10 dB is 5.47-6.13 GHz. In comparison, the traditional single-feed Antenna 1 (probe feed) has a simulated AR bandwidth of 5.77-5.87 GHz (1.7%). The traditional dual-feed Antenna 2 (proximity coupling) has a simulated AR bandwidth of 5.72-5.83 GHz (1.9%). In addition, both two reference antennas have only one AR minimum, this means that only one CP mode is radiated on each reference antenna. Compared to these reference antennas, the AR bandwidth improvement is obvious and spectacular. At least 4.1 times (=7.8%/1.9%) wider AR bandwidth is achieved for the presented 1×2 CP array antenna.

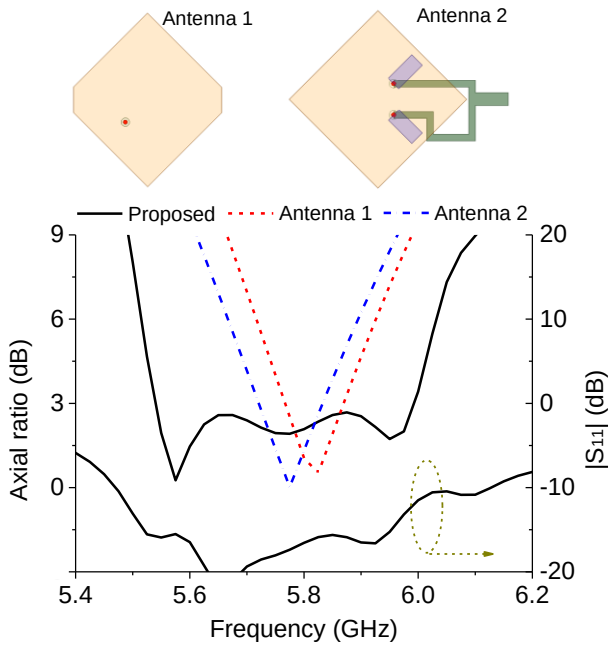

Fig. 7. Comparison to the traditionally designed single-feed CP antenna (Antenna 1) and dual-feed CP antenna (Antenna 2).

To illustrate the different CP radiation mechanism for the proposed antenna, Fig. 8 gives the current distributions on the surface of the radiating patches at different CP radiating modes and at different sweeping times. Note that in the figure, T_i (i=1, 2, and 3) is the oscillation period at different frequencies of 5.58, 5.78, and 5.95 GHz.

As shown in Fig. 8 (a), for the first CP mode at 5.58 GHz, the input energy is mainly transmitted to the second dual-feed CP antenna, and strong current magnitude can be observed on the surface of the dual-feed square patch. This means that the first CP mode is mainly controlled by the radiation on the right dual-feed square patch. For the center CP mode at 5.78 GHz shown in Fig. 8 (b), both the left and right patches are observed with strong current magnitudes. Most importantly, the current directions on the two patches are synchronous and in the same direction as the time flows. This denotes that because of the coupling of two patches, the CP radiations on the two patches are synchronized with each other and form the center CP mode at this frequency. For the third CP mode at 5.95 GHz shown in Fig. 8 (c), strong current magnitude is primarily located on the surface of the left sing-feed patch, and week current is observed on the right patch. So the third CP mode is mainly controlled by the radiation on the left patch. In addition, observing from Fig. 8 (a) to Fig. 8 (c), it can be found that as the time flows, the surface currents at different CP modes are all rotated in the same right-hand direction. Therefore, RHCP radiation is realized for the proposed 1×2 CP array antenna.

Fig. 9 shows the different effects of key design parameters on the AR performance of the proposed 1×2 array antenna. In the antenna design, the length of the right square patch (L4), the length of the left chamfered patch (L1), and the length of chamfered corner (L3) have great and different effects on the three CP modes. So they are studies here for the convenience of antenna design. As shown in Fig. 9 (a), when the length of the right square patch is increased from 16.8 mm to 17.2 mm, the first CP mode moves to the lower frequency obviously, which causes the left AR boundary line moves substantially to the left. The second and third CP modes are only slightly changed, and the right boundary lines are nearly overlapped. This confirms that the first CP mode is mainly controlled by the radiation on the right square patch.

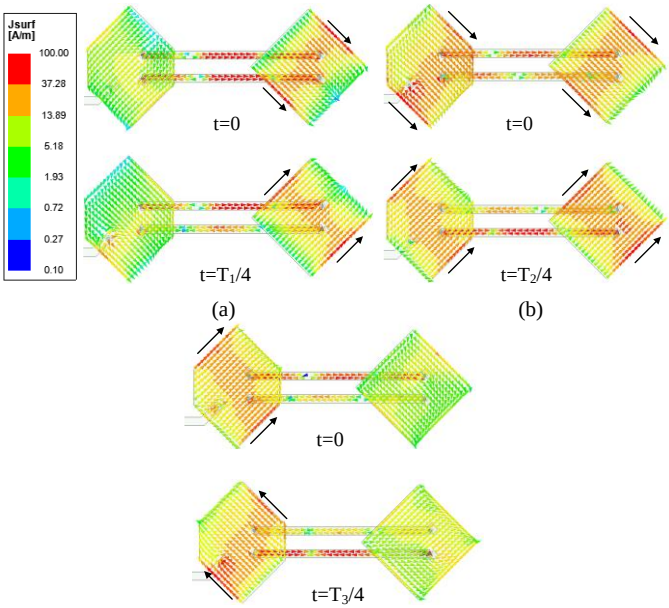

Fig. 8. Current distributions on the surface of the proposed 1×2 CP array antenna at different frequencies. (a) 5.58 GHz, (b) 5.78 GHz, and (c) 5.95 GHz.

Fig. 9 (b) shows the simulated AR varies with different lengths of the left patch (L1). It can be seen that the third CP modes moves substantially to the lower frequencies as the increase of L1, while the first CP mode and the left AR boundary line are nearly unaffected. It should be noted that, as the change of the third CP mode, the center CP mode is also slightly affected and moves to the lower frequency. As studied in Section II, the length of the chamfered corner (L3) has an important effect on the performance of HP-QPD, and it also can have a great effect on the AR performance of the presented array antenna. Fig. 9 (c) shows the radiated AR varying with different lengths of L3. It can be seen that the variance of L3 can affect all the CP modes. When the length of the chamfered

corner is increased, both the first and third CP modes move to the lower frequency, and this causes the whole AR bandwidth move to the lower frequency. This is because that L3 can not only affect the CP mode on the left patch, but also affect the quadrature output to the right patch as illustrated in Section II. Therefore, the whole AR bandwidth can be affected as the change of L3. Finally, based on the above key parametrical studies, it is not difficult to design a wideband CP antenna by using the presented method.

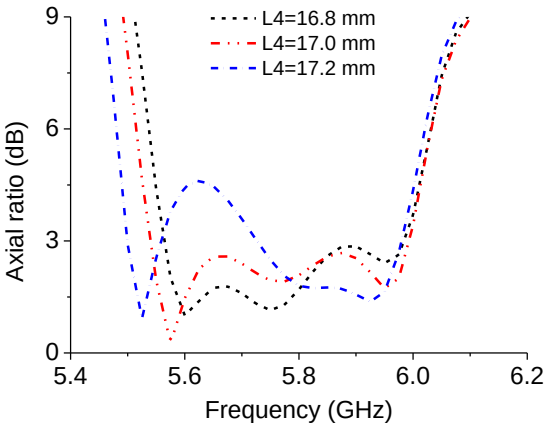

(a)

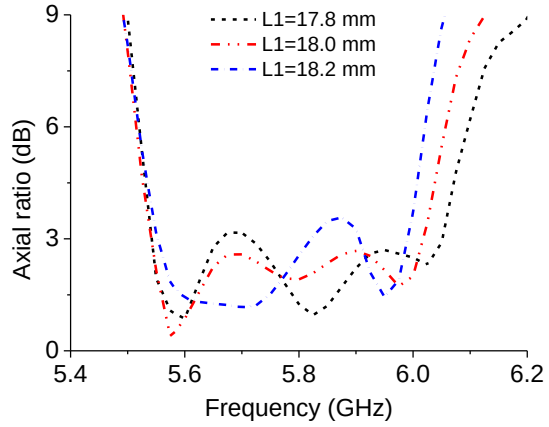

(b)

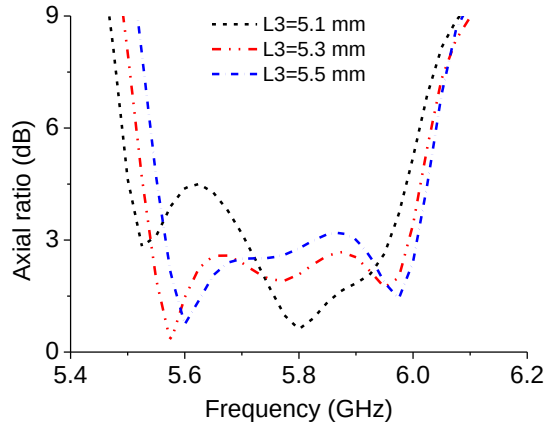

(c)

Fig. 9. The effects of different parameters on the AR performance of the proposed 1×2 CP array antenna. (a) Length of the square patch (L4). (b) Length of the chamfered patch (L1). (c) Length of the chamfered corner (L3).

Other parameters, such as the length and width of the ground plane, can also have a slight effect on the performance of this 1×2 array antenna. Due to the asymmetry of the ground plane, when the ground size is largely changed, its radiated AR will be affected. However, its impedance bandwidth is nearly unaffected. In the simulation, it is found that the effect caused by the ground size is less sensitive to parameters of L4, L1, and L3. Therefore, more careful consideration needed to be taken into the parametrical studies shown in Fig. 9.

C. Results

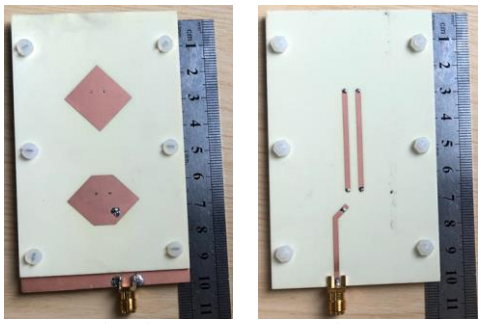

Fig. 10. Photographs of the fabricated prototype of the presented 1×2 CP array antenna.

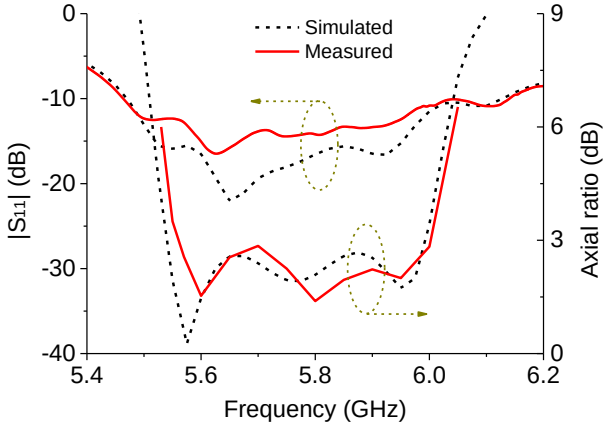

Fig. 11. Measured and simulated S-parameters and axial ratios of the presented 1×2 CP array antenna.

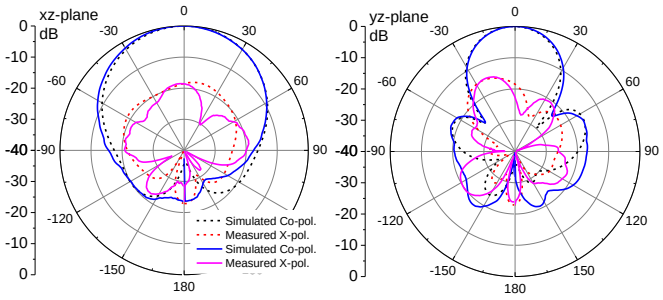

Fig. 12. Measured and simulated normalized radiation patterns of the 1×2 CP array antenna at 5.8 GHz.

The proposed 1×2 CP array antenna was fabricated and measured for the final performance verification, and the photographs of the fabricated prototype are shown in Fig. 10. Fig. 11 gives the measured S-parameters and AR, which are compared with the simulated results. Note that in this work, the measured S-parameters are obtained by Anritsu 37397C vector network analyzer, and the measured far-field results are obtained by the anechoic chamber at the University of Kent. It

can be seen that the measured impedance bandwidth for $|S_{11}|$<-10 dB is 5.46-6.14 GHz, and the measured CP bandwidth for AR<3 dB is 5.56-6.02 GHz. The measured results agree well with the simulated results with a slight frequency shift to the upper frequency.

Fig. 12 gives the measured normalized radiation patterns of the fabricted 1×2 CP array antenna at 5.8 GHz. It can be seen that the measured radiation patterns agree well with the simulated radiation patterns. Note that for the radiation patterns, right-hand CP radaition is the co-polarization, and left-hand CP radaition is the cross-polarization. The discrepencies between the meausred and simulated radiation patterns are mainly caused by influence from the feed cable, auxiliary fixtures, and position errors in measurement. In addition, the operational bandwidth shift can also cause the cross-polarization level being increased or reduced. The meausred half-power beamwidth for co-polarized radiation patterns is around 70° in xz-plane, and 36° in yz-plane within the bandwidth. Owing to the large ground size, high front-to-back ratio of 18.6 dB is achieved within the bandwidth. The measured peak realized gain is around 10.2 dBic within the CP bandwidth.

IV. 1×8 CP ARRAY ANTENNA

A. Array Configuration

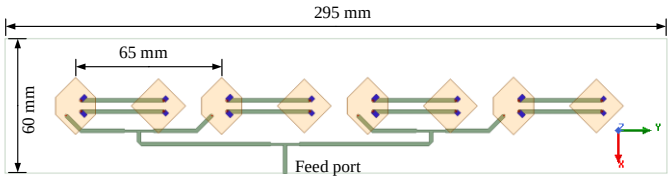

Fig. 13. Configuration of the proposed wideband CP 1×8 array antenna.

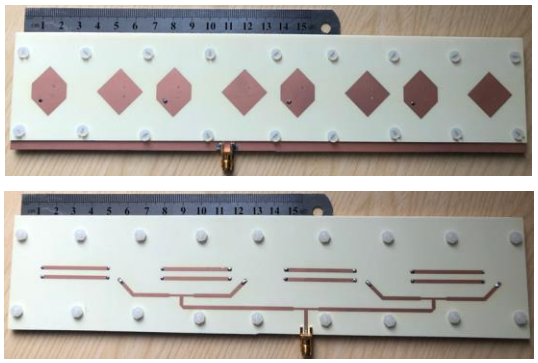

Fig. 14. Photographs of the fabricated prototype of 1×8 CP array antenna.

To realize high gain CP radiation, another 1×8 array antenna using the proposed element is designed. Fig. 13 shows the detailed configuration of this high gain CP array antenna. As can be seen, four same 1×2 array elements are linearly arranged in x-axis direction with the average element distance of 32.5mm, which is 0.63 λ_0 (where λ_0 is the free space wavelength at 5.8 GHz). Note that the 1×8 array antenna keeps the same layer configuration as the 1×2 array antenna, and the entire size of the array antenna is 295 mm×60 mm. A T-typed splitter is used as the simple feed network for equal magnitude distribution, which is designed on the bottom layer of the substrate with a symmetrical structure. A SMA connector is connected to the end of the T-typed power divider for all the performance measurements.

B. Results

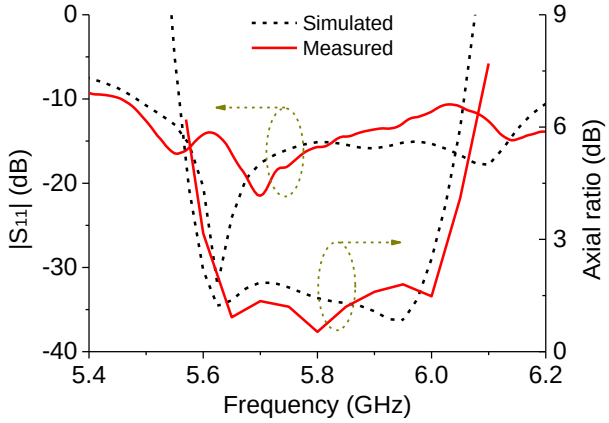

Fig. 15. Measured and simulated S-parameters and ARs of the fabricated 1×8 CP array antenna.

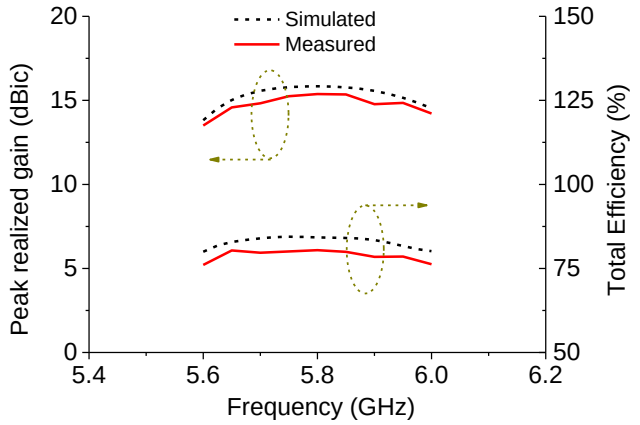

Fig. 16. Measured and simulated peak realized gains and total efficiencies of the fabricated 1×8 CP array antenna.

Fig. 14 shows the photographs of the fabricated prototype of 1×8 CP array antenna. Fig. 15 gives the measured S_{11} and AR of the linear array antenna, and the simulated results are also shown for a good comparison. It can be seen that the measured impedance bandwidth of the 1×8 array for $|S_{11}|$<-10 dB is 5.46-6.2 GHz, which is slightly wider than the simulated S_{11}. The measured CP bandwidth for AR<3 dB is 5.61-6.04 GHz, which has a slight frequency shift to the upper frequency compared to the simulated AR curve. Both the measured and simulated results have a good accordance.

The gain and radiation patterns of the 1×8 array antenna were also measured in the anechoic chamber. Fig. 16 shows the measured peak realized CP gain and total efficiency of the linear array. It can be seen that high radiation gain is achieved for the fabricated array antenna. The measured highest peak realized gain is 15.4 dBic within the bandwidth. Stable total efficiency (including the impedance mismatch loss) is obtained with the value around 79% within the bandwidth. The measured and simulated normalized radiation patterns at 5.65 GHz, 5.8 GHz, and 5.95 GHz are shown in Fig. 17. It can be observed that the measured co-polarized radiation patterns agree well with the simulated radiation patterns, especially for the patterns within the beamwidth. It is observed that there are some differences between simulated and measured

cross-polarized radiation patterns. These differences are mainly caused by the effect of feed coaxial cable, supporting fixtures, and position errors. In addition, the cross-polarization level can also be affected by the frequency band shift due to the substrate instability and fabrication errors. The measured half-power beamwidth in xz-plane is around 68°, and the beamwidth in yz-plane is around 10° within the bandwidth. High front-to-back ratio is achieved with the value higher than 22.5 dB.

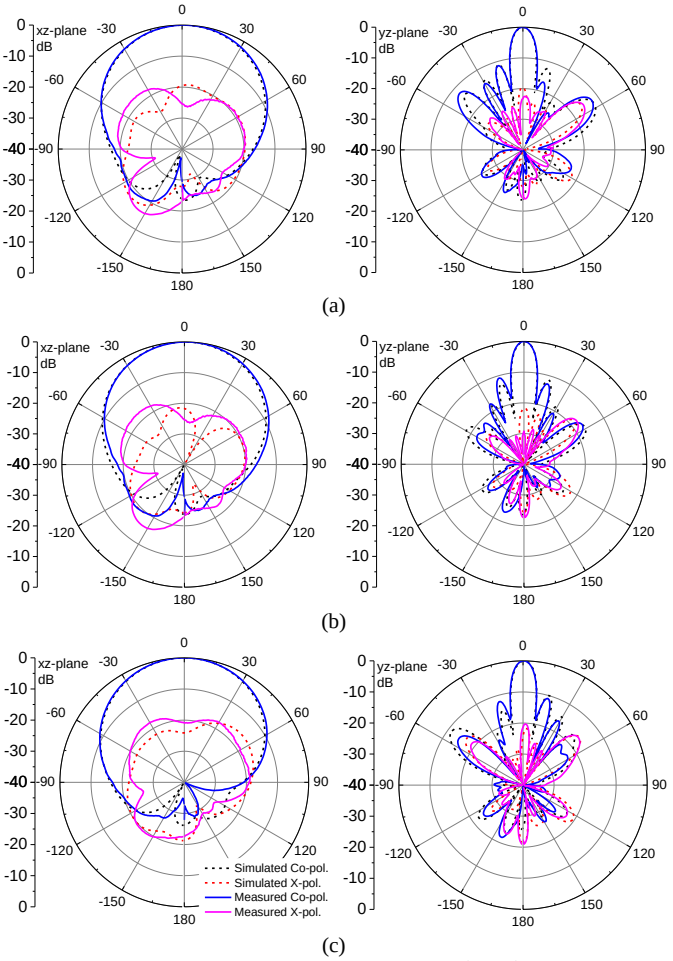

Fig. 17. Measured and simulated radiation patterns of the fabricated 1×8 CP array antenna at (a) 5.65 GHz, (b) 5.8 GHz, and (c) 5.95 GHz.

C. Comparison

Table I compares the presented array antennas with the recently published CP patch antennas. In the table, λ_0 is the free space wavelength at the center operation frequency. Compared to [13], [15], [17], and [23], the proposed antenna arrays keep low profile and compact size, but have a wider overlapped impedance and AR bandwidth. The CP antenna in [18] uses eight parasitic patches for bandwidth improvement, so it has a wide AR bandwidth of 12.9% and high antenna gain with a thin substrate thickness. However, due to the introduced eight parasitic patches, large radiator size of around $0.7\lambda_0\times0.7\lambda_0$ and tilted radiation patterns are observed within the bandwidth, which makes the antenna element difficult to be extended into array designs for high gain unidirectional radiation. By combining an integrated sequentially rotated feed network and a Wilkinson power divider for broadband CP radiation, the 2×5 array antenna in [21] has an enhanced CP bandwidth of 12.5% with a thin thickness of $0.054\lambda_0$. However, this combination could incur a high insertion loss and low antenna gain. This 10-element array antenna is observed with a low antenna gain of 10.7 dBic and tilted unsymmetrical beams. While our presented 2-element linear array antenna has a peak realized gain of 10.2 dBic, and the 8-element linear array antenna has a peak realized gain of 15.4 dBic.

The antenna area of each reference antenna is added in the table for comparison. As can be seen, the average area of a single antenna element is around $1\lambda_0\times1\lambda_0$. When the antenna is expanded into array design, the size of total array antenna will be increased according to its element distance. The proposed two antenna arrays have average areas for CP radiation, but own low profile and wide operation bandwidth. Observing from both the simulated and measured results, the performances of the proposed 1×8 array antenna have a good consistency with its array element, so it can be easily expanded into a large-scale array design with a simple feed network.

TABLE I
COMPARISON OF THE RECENTLY PUBLISHED CIRCULARLY POLARIZED PATCH ANTENNAS

Ref.	Overlapped BW (GHz)	RBW	Thickness (λ_0)	Element	Area ($\lambda_0\times\lambda_0$)	Peak Gain (dBic)
[13]	3.25-3.41	4.8%	0.033	1	2.22×1.33	5.8
[15]	5.02-5.34	6.2%	0.041	1	0.95×0.95	7.0
[17]	4.86-5.12	5.2%	0.058	2×2	1.66×1.66	10.5
[18]	5.38-6.12	12.9%	0.029	1	0.96×0.96	9.8
[21]	4.95-5.61	12.5%	0.054	2×5	1.64×3.43	10.7
[23]	7.4-7.7	4%	0.068	4×4	2.77×2.77	14
Proposed	5.56-6.02	7.9%	0.031	1×2	1.16×1.93	10.2
	5.61-6.04	7.4%	0.031	1×8	1.16×5.69	15.4

V. CONCLUSION

This paper proposes a novel method of designing low-profile wideband CP array patch antennas using an integrated HP-QPD. First, HP-QPD is proposed and discussed in detail. Analyses show that it can radiate half-power CP waves and output the remaining half-power with equal magnitude and quadrature phase difference. Therefore, based on this novel characteristic, a 1×2 CP array antenna is designed with a simple feed network and a compact size. In addition, a wide AR bandwidth with three CP modes is achieved for the presented 1×2 array antenna. A 1×8 CP array antenna is further designed for high gain CP radiation. Both two array antennas were fabricated and measured for the final performance verification. Results show that the measured overlapped impedance and AR bandwidth of 1×2 and 1×8 CP array antennas are 7.9% and 7.4% respectively. Both two antennas have a good consistency in the impedance and radiation performances. Therefore, the presented array antennas can be a good candidate for wireless communication systems.

REFERENCES

[1] S. Gao, Q. Luo, and F. Zhu, *Circularly polarized antennas.* J Hoboken, NJ, USA: Wiley, 2013.

[2] L. Wen, S. Gao, Q. Luo, W. Hu, and B. Sanz-Izquierdo, "Design of a broadband circularly polarized antenna by using axial ratio contour," *IEEE Antennas Wireless Propag. Lett.*, vol. 19, no. 12, pp. 2487-2491, Dec. 2020.
[3] Y. Luo, Q. Chu, and L. Zhu, "A low-profile wide-beamwidth circularly-polarized antenna via two pairs of parallel dipoles in a square contour," *IEEE Trans. Antennas Propag.*, vol. 63, no. 3, pp. 931-936, March 2015.
[4] R. Xu, J. Li, and W. Kun, "A broadband circularly polarized crossed-dipole antenna," *IEEE Trans. Antennas Propag.*, vol. 64, no. 10, pp. 4509-4513, Oct. 2016.
[5] H. D. Li, X. Y. Du, J. Y. Yin, J. Ren, and Y. Yin, "Differentially fed dual-circularly polarized antenna with slow wave delay lines," *IEEE Trans. Antennas Propag.*, vol. 68, no. 5, pp. 4066-4071, May 2020.
[6] L. Wen, S. Gao, Q. Luo, W. Hu, and Y. Yin, "Wideband dual circularly polarized antenna for intelligent transport systems," *IEEE Trans. Veh. Technol.*, vol. 69, no. 5, pp. 5193-5202, May 2020.
[7] L. Wen et al., "A wideband series-fed circularly polarized differential antenna by using crossed open slot-pairs," *IEEE Trans. Antennas Propag.*, vol. 68, no. 4, pp. 2565-2574, April 2020.
[8] R. Xu et al., "Analysis and design of ultrawideband circularly polarized antenna and array," *IEEE Trans. Antennas Propag.*, vol. 68, no. 12, pp. 7842-7853, Dec. 2020.
[9] L. Wen, S. Gao, Q. Luo, W. Hu, and B. Sanz-Izquierdo, "Design of a wideband dual-feed circularly polarized antenna for different axial ratio requirements," *IEEE Antennas Wireless Propag. Lett.,* vol. 20, no. 1, pp. 88-92, Jan. 2021.
[10] W. Hu et al., "Wideband circularly polarized antenna using single-arm coupled asymmetric dipoles," *IEEE Trans. Antennas Propag.,* vol. 68, no. 7, pp. 5104-5113, July 2020.
[11] N. Nasimuddin, Y. S. Anjani, and A. Alphones, "A Wide-beam circularly polarized asymmetric-microstrip antenna," *IEEE Trans. Antennas Propag.,* vol. 63, no. 8, pp. 3764-3768, Aug. 2015.
[12] C. S. Lee, Y. Fan, and M. Ezzat, "Single-feed circularly polarized microstrip antenna with bethe holes on the radiating patch," *IEEE Trans. Antennas Propag.*, vol. 68, no. 6, pp. 4935-4938, June 2020.
[13] N.-W. Liu, L. Zhu, Z.-X. Liu, G. Fu, and Y. Liu, "Design approach of a single circularly polarized patch antenna with enhanced AR-bandwidth under triple-mode resonance," *IEEE Trans. Antennas Propag.*, vol. 68, no. 8, pp. 5827-5834, Aug. 2020.
[14] C. Mao, S. S. Gao, Y. Wang, and J. T. Sri Sumantyo, "Compact broadband dual-sense circularly polarized microstrip antenna/array with enhanced isolation," *IEEE Trans. Antennas Propag.*, vol. 65, no. 12, pp. 7073-7082, Dec. 2017.
[15] Q. Wu, X. Zhang, and L. Zhu, "A wideband circularly polarized patch antenna with enhanced axial ratio bandwidth via co-design of feeding network," *IEEE Trans. Antennas Propag.,* vol. 66, no. 10, pp. 4996-5003, Oct. 2018.
[16] Z. H. Jiang and D. H. Werner, "A compact, wideband circularly polarized co-designed filtering antenna and its application for wearable devices with low SAR," *IEEE Trans. Antennas Propag.,* vol. 63, no. 9, pp. 3808-3818, Sept. 2015.
[17] Y. Li, Z. Zhang, and Z. Feng, "A sequential-phase feed using a circularly polarized shorted loop structure," *IEEE Trans. Antennas Propag.*, vol. 61, no. 3, pp. 1443-1447, March 2013.
[18] K. Ding, C. Gao, D. Qu and Q. Yin, "Compact broadband circularly polarized antenna with parasitic patches," *IEEE Trans. Antennas Propag.*, vol. 65, no. 9, pp. 4854-4857, Sept. 2017.
[19] K. L. Lau and K. M. Luk, "A novel wide-band circularly polarized patch antenna based on L-probe and aperture-coupling techniques," *IEEE Trans. Antennas Propag.,* vol. 53, no. 1, pp. 577-582, Jan. 2005.
[20] L. Bian, Y.-X. Guo, L.-C. Ong and X.-Q. Shi, "Wideband circularly polarized patch antenna," *IEEE Trans. Antennas Propag.*, vol. 54, no. 9, pp. 2682-2686, Sept. 2006.
[21] Y. Shen, S. Zhou, G. Huang and T. Chio, "A compact dual circularly polarized microstrip patch array with interlaced sequentially rotated feed," *IEEE Trans. Antennas Propag.,* vol. 64, no. 11, pp. 4933-4936, Nov. 2016.
[22] Y. Yang, J. Guo, B. Sun, Y. Cai, and G. Zhou, "The design of dual circularly polarized series-fed arrays," *IEEE Trans. Antennas Propag.,* vol. 67, no. 1, pp. 574-579, Jan. 2019.
[23] C. Mao, Z. H. Jiang, D. H. Werner, S. S. Gao, and W. Hong, "Compact self-diplexing dual-band dual-sense circularly polarized array antenna with closely spaced operating frequencies," *IEEE Trans. Antennas Propag.*, vol. 67, no. 7, pp. 4617-4625, July 2019.
[24] S. Ogurtsov and S. Koziel, "A conformal circularly polarized series-fed microstrip antenna array design," *IEEE Trans. Antennas Propag.*, vol. 68, no. 2, pp. 873-881, Feb. 2020.

Lehu Wen received Ph.D. degree in electronic engineering from the University of Kent, Canterbury, U.K, in 2020.

He is currently a Research Associate with the School of Engineering and Digital Arts, University of Kent, Canterbury, U.K. His research interests include wideband dual-polarized antennas, circularly polarized antennas, tightly coupled array antennas, and mobile terminal antennas.

Steven Gao (Fellow, IEEE) received the Ph.D. degree in microwave engineering from Shanghai University, Shanghai, China, in 1999.

He is currently a Full Professor and Chair in RF and Microwave Engineering, and the Director of Graduate Studies at the School of Engineering and Digital Arts, University of Kent, UK. His current research interests include smart antennas, phased arrays, MIMO, satellite antennas, satellite communications, UWB radars, synthetic aperture radars, and mobile communications. He is currently an Associate Editor of the IEEE TRANSACTIONS ON ANTENNAS AND PROPAGATION.

Qi Luo (Senior Member, IEEE) is currently a Senior Lecturer with the School of Physics, Engineering and Computer Science, University of Hertfordshire, Hatfield, U.K.

Wei Hu (Member, IEEE) is currently an Associate Professor with the National Key Laboratory of Antennas and Microwave Technology, Xidian University, Xi'an, China.

Benito Sanz-Izquierdo is currently a Senior Lecturer with the School of Engineering and Digital Arts, University of Kent, Canterbury, U.K.

Xue-Xia Yang (Senior Member, IEEE) is currently a Professor with the School of Communication and Information Engineering, Shanghai University, Shanghai, China.